Accretion Disks Around Binary Black Holes: A Quasistationary Model

Yuk Tung Liu[1] and Stuart L. Shapiro[1,*]

[1]*Department of Physics, University of Illinois at Urbana-Champaign, Urbana, IL 61801*

Tidal torques acting on a gaseous accretion disk around a binary black hole can create a gap in the disk near the orbital radius. At late times, when the binary inspiral timescale due to gravitational wave emission becomes shorter than the viscous timescale in the disk, the binary decouples from the disk and eventually merges. Prior to decoupling the balance between tidal and viscous torques drives the disk to a quasistationary equilibrium state, perturbed slightly by small amplitude, spiral density waves emanating from the edges of the gap. We consider a black hole binary with a companion of smaller mass and construct a simple Newtonian model for a geometrically thin, Keplerian disk in the orbital plane of the binary. We solve the disk evolution equations in steady state to determine the quasistationary, (orbit-averaged) surface density profile prior to decoupling. We use our solution, which is analytic up to simple quadratures, to compute the electromagnetic flux and approximate radiation spectrum during this epoch. A single nondimensional parameter $\tilde{g}$, equal to the ratio of the tidal to viscous torque at the orbital radius, determines the disk structure, including the surface density profile, the extent of the gap, the existence of an inner disk, and the accretion rate. The solution reduces to the Shakura-Sunyaev profile for a stationary accretion disk around a single black hole in the limit of small $\tilde{g}$. Our solution may be useful for choosing physical parameters and setting up quasistationary disk initial data for detailed numerical simulations that begin prior to decoupling and track the subsequent evolution of a black hole binary-disk system.

PACS numbers: 98.62.Mw, 98.62.Qz

I. INTRODUCTION

Binary black hole (BHBH) mergers typically occur in regions immersed in gas, and the capture and accretion of the gas by the binary may result in appreciable electromagnetic radiation. Following the detection of gravitational waves from a BHBH merger, electromagnetic "afterglow" radiation could provide confirmation of the coalescence [1–7]. Such electromagnetic radiation can also serve as a useful probe of the gas in galaxy cores or in other regions where mergers take place, as well as a diagnostic of the physics of black hole accretion. The timescale during which detectable "afterglow" radiation achieves its maximum value occurs when the gas is driven close to the remnant and ranges from several years to tens of decades in the case of supermassive BHBH systems with total masses of $10^5 - 10^8 M_\odot$. Together with detecting the gravitational waves, observing this electromagnetic radiation may even provide a means of witnessing the birth of a quasar [8].

There is also the possibility of detecting electromagnetic "precursor" radiation prior to the merger and before the maximum gravitational wave emission [9, 10]. If the distant gas is nearly homogeneous and either at rest with respect to the binary ("binary Bondi" accretion) or moving ("binary Bondi-Hoyle-Lyttleton" accretion) and optically thin, the luminosity will peak at the end of the binary inspiral phase immediately prior to the final plunge [11]. At this stage shock heating of the gas and turbulent magnetic field amplification is strongest. The peak luminosity lasts for $\delta t \sim M_6$ hours prior to merger and then plummets sharply following the coalescence. Here M_6 is the binary mass in units of $10^6 M_\odot$. If, instead, the accretion takes place via a geometrically-thin, optically-thick Keplerian disk around the binary ("binary Shakura-Sunyaev" accretion), there may be a late-time precursor brightening from tidal and viscous (or turbulent magnetic) dissipation in the inner disk. This radiation peaks on a timescale $\delta t \sim 0.1 M_6$ days prior to merger and it remains high afterwards [10].

In this paper we focus on geometrically thin disks prior to disk-binary decoupling and well before any late-time brightening of the "precursor" electromagnetic radiation. Our calculations are based on a simplified, Newtonian prescription for a Keplerian disk in the orbital plane of a binary BHBH system with a low mass ratio. Similar disk equations have been integrated previously in time to follow the (secular) evolution of such a BHBH-disk system for selected cases (see. e.g., [9, 10]). Here we adopt the equations to solve for steady state. We then apply our solution to determine the orbit-averaged disk structure and electromagnetic radiation during the inspiral epoch prior to decoupling, when our quasistationary approximation is appropriate.

Our simple treatment determines the quasistationary, orbit-averaged, surface density profile $\Sigma(r)$ of the circumbinary disk prior to decoupling, as well as the accretion rate, luminosity and approximate spectrum of the electromagnetic radiation. Our semi-analytic analysis, (i.e. analytic up to simple quadratures), serves to identify some of the key physical parameters that determine these quantities. Several nondimensional parameters fix the overall shape of the density profile. Among these pa-

*Also Department of Astronomy and NCSA, University of Illinois at Urbana-Champaign, Urbana, IL 61801

rameters are the binary mass ratio q, assumed small, the ratio of the disk scale height to radius, h/r, also small, in the ring-like gap in the disk at the orbital radius of the secondary, and the power-law n defining the variation of the disk viscosity with radius, $\nu \propto r^n$. Other parameters, such as the total binary mass M, determine the physical scale of the disk and, together with the accretion rate $\dot{M}$, the characteristic luminosity and frequency of the emitted radiation.

We find that many of the properties of the disk, such as the surface density profile, the extent of the gap at the orbit of the secondary, the existence of an inner disk and the accretion rate, are determined by a single nondimensional parameter $\tilde{g}$. This parameter is essentially the ratio of the tidal to viscous torque at the orbital radius.

A reliable description of the accretion flow and associated radiation from a merging BHBH binary really requires a radiation magnetohydrodynamics simulation in full general relativity in a $3+1$-dimensional, dynamical spacetime. Such simulations have yet to be performed in any detail. However, Newtonian hydrodynamic simulations incorporating some of the relevant physics have been performed at various levels of approximation (see, e.g., [2, 4, 5, 12]) and general relativistic simulations are underway (e.g., [11, 13–17]). The model discussed here, although based on a simplified description, can help select input parameters and identify scaling behavior for such simulations. In addition, the resulting quasistationary description of the disk provides approximate initial data for numerical simulations that begin prior to binary-disk decoupling.

We adopt geometrized units and set $G = 1 = c$ below.

II. BASIC MODEL

A. Timescales and Overview

There are several characteristic timescales that determine the structure of a gaseous disk in a BHBH system. The orbital timescale in a Keplerian disk with orbital angular frequency $\Omega_K(r) = (M/r^3)^{1/2}$ is given by

$$t_{\rm orb}(r) = 2\pi \left(\frac{r^3}{M}\right)^{1/2} , \qquad (1)$$

where r is local disk radius. The viscous timescale is given by

$$t_{\rm vis}(r) = \frac{\Sigma}{(d\Sigma/dt)_{\rm vis}} \approx \frac{M_{\rm disk} r^2 \Omega_K(r)}{T_{\rm vis}} \approx \frac{2}{3}\frac{r^2}{\nu} , \qquad (2)$$

where ν is the shear viscosity, $T_{\rm vis}$ is the viscous torque and $M_{\rm disk} \sim r^2\Sigma(r)$ is the disk mass. The timescale associated with the gravitational tidal torque on the disk due to the companion is

$$t^{\rm disk}_{\rm tid}(r) = \frac{\Sigma}{(d\Sigma/dt)_{\rm tid}} \approx \frac{M_{\rm disk} r^2 \Omega_K(r)}{T_d}, \qquad (3)$$

where T_d is the gravitational tidal torque. The inspiral timescale of the binary due to the emission of gravitational waves is

$$t_{\rm GW}(a) = \frac{a}{(da/dt)_{\rm GW}} = \frac{5}{16}\frac{a^4}{M^3\zeta} , \qquad (4)$$

where a is the binary separation and $\zeta \equiv 4q/(1+q)^2$. Finally, the binary orbit is also changed by the torque exerted by the disk on the secondary of mass $m = qM$. The timescale is

$$t^m_{\rm tid} = \frac{a}{(da/dt)_{\rm tid}} \approx \frac{m a^2 \Omega_K(a)}{T_d} \approx \frac{m}{M_{\rm disk}} t^{\rm disk}_{\rm tid}(a). \qquad (5)$$

The inequality $t_{\rm orb}(r) \ll t_{\rm vis}(r)$ is satisfied throughout the disk at all times. For most of its history, the disk evolves on a slow, secular, viscous timescale and not on a rapid dynamical timescale [18]; viscosity maintains the gas in nearly Keplerian circular orbits. In a quasistationary state, where the effects of viscosity and tidal torques balance each other, we have $t^{\rm disk}_{\rm tid} \sim t_{\rm vis}$. Consider the typical case where the disk mass satisfies $M_{\rm disk} \ll m$. It follows from Eq. (5) that $t^{\rm disk}_{\rm tid}(a) \ll t^m_{\rm tid}$. Hence, as long as the disk is quasistationary, we have $t_{\rm vis}(a) \ll t^m_{\rm tid}$. However, $t^m_{\rm tid}$ can be longer or shorter than $t_{\rm GW}$ during the early inspiral history. Prior to decoupling, even as the binary separation shrinks due to the combined effects of gravitational radiation and tidal torque back-reaction, the orbital separation always remains momentarily "frozen" while the disk adjusts to tidal-viscous torque balance to maintain quasiequilibrium. Eventually, as the binary inspirals further, the timescale due to gravitational wave emission becomes shorter than the viscous timescale and the binary decouples from the disk [1, 9, 19]. We note that as long as $M_{\rm disk}/m \ll 1$, $t_{\rm vis} \ll t^m_{\rm tid}$ holds. Hence at decoupling and thereafter, the orbital decay is driven by gravitational radiation, not the torque of the disk. Quasiequilibrium no longer applies after decoupling.

The orbital radius at which decoupling begins can be estimated from the relation $t_{\rm GW}(a) \sim \beta t_{\rm vis}(2\lambda a)$. Here $\lambda \equiv r/2a \sim 1$ is the nearly constant ratio between the disk edge and the orbital separation prior to decoupling and is determined by a balance between viscous stresses in the disk and gravitational tidal torques from the binary [12, 20]. The parameter $\beta \sim 0.1$ roughly accounts for the shortening of the viscous timescale at the edge where the surface density Σ is very steep [21]. An α-disk with a viscosity law $\nu(r) = (2/3)\alpha P_{\rm gas}/(\rho\Omega_{\rm K})$, where ρ is the gas density and $P_{\rm gas}$ is the gas pressure, yields a decoupling radius a_d given by [1, 7]

$$\frac{a_{\rm d}}{M} \approx 126\alpha_{-1}^{-17/50} S^{-49/200} \lambda^{7/10} M_6^{2/25} (\beta_{-1}\zeta)^{17/40} \theta_{0.2}^{-17/200} , \qquad (6)$$

where $\alpha = 0.1\alpha_{-1}$, $\beta = 0.1\beta_{-1}$, $S \equiv 3\pi\Sigma(a_{\rm d})\nu(a_{\rm d})/\dot{M}_{\rm Edd}$ and $\theta = 0.2\theta_{0.2}$. Here $\dot{M}_{\rm Edd} = 4\pi M m_p/(\eta\sigma_T)$ is the Eddington accretion rate, σ_T is the Thomson cross-section for electron scattering, η is the radiative efficiency and

$\theta < 1$ is a porosity correction factor applied to the scattering-dominated optical depth [22]. The radiative efficiency $\eta \equiv L_{\rm Edd}/\dot{M}_{\rm Edd}$ may be set to 1/12 for a Newtonian thin disk disk with an innermost stable circular orbit (ISCO) at $r_{\rm isco} = 6M$, the value appropriate for a nonspinning black hole.

Most earlier work has focused on the late binary epoch *following* decoupling when $a < a_d$. During this epoch the outer disk remains almost frozen until after binary inspiral and coalescence, at which point the disk diffuses inward and fills up the hollow (in the case of equal-mass black holes), or gap (in the case of a low-mass companion), on a (slow) viscous timescale (see, e.g., [6, 7] and references therein). Eventually the gas reaches the ISCO of the remnant black hole, where all torques and surface densities vanish in a first approximation. Ultimately the disk settles into steady-state equilibrium around the black hole remnant. In this paper we shall be concerned primarily in the early binary epoch *prior* to decoupling when $a > a_d$. As we have described, during this epoch it is the binary orbit that remains nearly frozen while the the disk adjusts to the combined tidal and viscous torques, the effects of which balance each other in steady state. Thus, up until the BHBH orbit reaches decoupling, the disk evolves quasistatically as the orbit shrinks.

Because $t_{\rm orb}(r) \ll t_{\rm vis}(r)$ over the entire history of a quasistationary disk, the disk radial velocity satisfies $v_r \ll r\Omega_K(r)$ and the full hydrodynamic equations reduce to secular (conservation) equations to describe the orbit-averaged evolution of a Keplerian thin disk [23]. While obtaining the spiral density wave perturbations induced by the tidal torques near the edge of the disk does require the full set of hydrodynamical equations, deducing the underlying orbit-averaged disk profile does not. For the epoch prior to decoupling these secular equations can be solved in steady state to give the quasisteady disk structure for each value of the separation $a > a_d$. We perform this calculation below in the low-mass limit where $q < 1$.

B. Key Equations

1. Disk Evolution

The evolution of a geometrically thin, nearly Keplerian disk is determined by combining the equation of mass conservation,

$$\frac{\partial \Sigma}{\partial t} + \frac{1}{r}\frac{\partial (r\Sigma v_r)}{\partial r} = 0 \tag{7}$$

with the equation of angular momentum conservation,

$$\frac{\partial (\Sigma r^2 \Omega)}{\partial t} + \frac{1}{r}\frac{\partial (r\Sigma v_r r^2 \Omega)}{\partial r} = \frac{1}{2\pi r}\frac{\partial G}{\partial r} \tag{8}$$

to obtain an evolution equation for the surface density, $\Sigma(t, r)$,

$$\frac{\partial \Sigma}{\partial t} = -\frac{1}{2\pi r}\frac{\partial}{\partial r}\left[\left(\frac{\partial (r^2\Omega)}{\partial r}\right)^{-1}\frac{\partial G}{\partial r}\right] . \tag{9}$$

Here $G \equiv -T_{\rm vis} + T_d$ is the total torque, $T_{\rm vis}$ is the viscous torque, T_d is the tidal torque on the disk from the presence of the secondary, and $\Omega = \Omega_K$ is the orbital frequency. The viscous torque density is given by the standard equation [9, 10, 23, 24]

$$\frac{\partial T_{\rm vis}}{\partial r} = -\frac{\partial}{\partial r}\left(2\pi r^3 \nu \Sigma \frac{\partial \Omega}{\partial r}\right) . \tag{10}$$

We approximate the (orbit-averaged) tidal torque density by using the expression adopted by Armitage and Natarajan [9]

$$\frac{\partial T_d}{\partial r} = 2\pi \Lambda \Sigma r \tag{11}$$

where $\Lambda(r, a)$ is given by

$$\Lambda = \begin{cases} -\left(fq^2 M/2r\right)\left(r/\Delta_p\right)^4, & r < a \\ +\left(fq^2 M/2r\right)\left(a/\Delta_p\right)^4, & r > a \end{cases} . \tag{12}$$

In Eq. (12) f is a dimensionless normalization factor and Δ_p is given by $\Delta_p = \max(|r - a|, h)$. Calibrating the above expression for the tidal field against high-resolution, hydrodynamical simulations in two-dimensions for a low-mass, black hole secondary interacting with an outer accretion disk, Armitage and Natarajan find that the value $f \approx 0.01$ best fits the simulation results. Equations (11) and (12) furnish a reasonable analytic approximation to the results obtained from summing over the pointlike contributions from the Lindblad resonances in the disk [25, 26]. (Similar, but slightly different, forms for the tidal torque also have been used in the literature; see, e.g., [10, 27–29]. For an analysis in general relativity, see [30, 31].) Assembling the above expressions then yields the final evolution equation

$$\frac{\partial \Sigma}{\partial t} = \frac{1}{r}\frac{\partial}{\partial r}\left[3r^{1/2}\frac{\partial}{\partial r}\left(r^{1/2}\nu\Sigma\right) - \frac{2\Lambda\Sigma r^{3/2}}{M^{1/2}}\right] . \tag{13}$$

The rate at which the secondary black hole migrates is determined both by back-reaction to the tidal torquing of the disk and by gravitational wave emission,

$$\dot{a} = \dot{a}_{\rm tid} + \dot{a}_{\rm GW} , \tag{14}$$

where

$$\dot{a}_{\rm tid} = -\frac{4\pi a^{1/2}}{M^{3/2} q}\int_{r_{\rm isco}}^{r_{\rm out}} r\Lambda\Sigma dr , \tag{15}$$

and where $a_{\rm GW}$ is given by Eq. (4). In Eq. (15) the integration is over the entire disk, although most of the

contribution from tidal torques arises close to the gap boundaries near $r \approx a$.

The accretion rate onto the primary may be calculated from

$$\begin{aligned} \dot{M}(t,r) &= 2\pi r\Sigma(-v_r), \\ &= -\left[\frac{(r^2\Omega)}{\partial r}\right]^{-1}\frac{\partial G}{\partial r}\ . \end{aligned} \tag{16}$$

Combining Eqs. (9) and (16) yields

$$\frac{\partial\Sigma}{\partial t} = \frac{1}{2\pi r}\frac{\partial}{\partial r}\dot{M}\ . \tag{17}$$

The coupled evolution Eqs. (13) and (14) have been integrated in time previously to explore select cases (see e.g. [9, 10]). Here we want to solve them for quasistationary flow in general. We will thereby obtain initial data for the construction of disks around low-mass binaries prior to decoupling that is valid in general cases. Thus we set $a =$ constant and $\partial\Sigma/\partial t = 0$ in Eq. (13) to obtain the density profile. According to Eq. (17) the resulting quasisteady accretion rate $\dot{M}$ is independent of r and can be obtained by solving Eq. (16) once the density profile has been determined.

In steady state, Eq. (13) becomes a second-order elliptic equation in r, for which we impose the following boundary conditions:

$$\text{b.c.'s}: \quad \nu\Sigma = \begin{cases} (\nu\Sigma)_{\rm out}, & r = r_{\rm out} \\ 0, & r = r_{\rm isco} \end{cases}\ . \tag{18}$$

In Eq. (18) $r_{\rm out}$ is the outer radius of the disk. We set the innermost stable circular orbit (ISCO) in the disk equal to $r_{\rm isco} = 6M$, the value appropriate for a nonspinning black hole remnant. Typically, $r_{\rm out} \gg r_{\rm isco}$ and in some cases we shall take $r_{\rm out} \to \infty$.

As mentioned above, the accretion rate $\dot{M}$ in steady state is independent of r. In steady state Eq. (13) admits a first integral which, when combined with Eq. (16) yields the first-order ODE

$$\dot{M} = 2\pi\left[3r^{1/2}\frac{d\left(r^{1/2}\nu\Sigma\right)}{dr} - \frac{2\Lambda\Sigma r^{3/2}}{M^{1/2}}\right] = \text{constant} \tag{19}$$

While we could solve the second-order Eq. (13) in steady state for the density profile, followed by Eq. (16) for the accretion rate, it is simpler to integrate the first-order Eq. (19). We do this in Sec. III A below.

2. Electromagnetic Radiation

The local radiated emission from the disk arises both from viscous and tidal dissipation. The rate of viscous dissipation per unit surface area is [23]

$$D_{\rm vis}(t,r) = \frac{9}{8}\nu\Sigma\frac{M}{r^3}. \tag{20}$$

The integrated rate of tidal dissipation may be obtained from the change in the binary binding energy due to tidal forces,

$$\dot{E}_{\rm tid}(t) = \frac{M^2 q}{2a}\left(\frac{|\dot{a}|}{a}\right)_{\rm tid}\ , \tag{21}$$

where $(\dot{a}/a)_{\rm tid}$ is given by Eq. (15). We follow [10] and assume that tidal dissipation results from the local damping of spiral density waves that mediate the binary-disk interaction and is thus proportional to the local generation of these waves,

$$D_{\rm tid}(t,r) = \frac{1}{4\pi r}\dot{E}_{\rm tid}\frac{|dT_d/dr|}{\int_{r_{\rm isco}}^{r_{\rm out}} dr|dT_d/dr|}\ . \tag{22}$$

Approximating the emission as thermal blackbody radiation, the local disk surface temperature $T_s(t,r)$ may be equated to the effective temperature, which is determined from the total dissipation rate $D = D_{\rm vis} + D_{\rm tid}$ according to

$$\sigma T_s^4(t,r) = D(t,r) \tag{23}$$

where σ is the Stefan-Boltzmann constant [32].

Given the surface temperature, the quasistationary specific flux $F_\nu(t)$ measured by an observer at distance d whose line of sight makes an angle i to the normal to the disk plane is determined by integrating over the entire disk surface,

$$F_\nu(t) = \frac{2\pi\,\cos i}{d^2}\int_{r_{\rm isco}}^{\infty} B_\nu(T_s(t',r))rdr, \tag{24}$$

where $B_\nu(T_s(t',r))$ is the Planck function, $t' = t - d$ is retarded time and ν is the photon frequency [33]. Equation (24) is best evaluated in terms of a nondimensional function $f^*(t',x)$ of nondimensional frequency x according to [6]

$$F_\nu(t) = \frac{2\pi\,\cos i}{d^2}\frac{15}{\pi^5}\frac{\sigma T_*^4}{\nu_*}r_{\rm isco}^2 f^*(t',x), \tag{25}$$

where

$$f^*(t',x) \equiv \int_1^\infty du\ u\frac{x^3}{\exp\left(xT_*/T_s\right) - 1}, \tag{26}$$

and where we have introduced the parameters

$$\begin{aligned} \sigma T_*^4 &\equiv 3M\dot{M}_{\rm rem}/8\pi r_{\rm isco}^3, \quad h\nu_* \equiv kT_*, \\ x &\equiv h\nu/kT_* = \nu/\nu_*, \quad u \equiv r/r_{\rm isco}. \end{aligned} \tag{27}$$

Here $\dot{M}_{\rm rem} = 3\pi(\nu\Sigma)_{\rm out}$ is the stationary accretion rate of an infinite disk onto the remnant black hole following merger [see Eq. (31)]. The quantity T_* provides a convenient estimate of the characteristic temperature in the main radiating region near $r_{\rm isco}$ of the final equilibrium disk following merger, and $h\nu_*$ is the characteristic

frequency of the emitted thermal radiation from this region. The specific luminosity $L_\nu(t)$, summing over both surfaces of the disk, is related to $F_\nu(t)$ according to

$$L_\nu(t) = \frac{2\pi d^2}{\cos\, i} F_\nu(t). \tag{28}$$

The total luminosity $L(t)$ integrated over all frequencies is then given by

$$L(t) = \int_0^\infty d\nu L_\nu(t) = \frac{60}{\pi^3}\sigma T_*^4 r_{\rm isco}^2 \int_0^\infty f^*(t', x) dx \tag{29}$$

Given the quasistationary density profile, we wish to perform these quadratures for the quasistationary electromagnetic spectrum prior to decoupling. Equation (29) yields

$$L = 2\int_{r_{\rm isco}}^{r_{\rm out}} D_{\rm vis} 2\pi r dr + \dot{E}_{\rm tid}\ . \tag{30}$$

We note that the final stationary equilibrium disk following merger yields well-known analytic density and temperature profiles, as well as analytic integrated fluxes and luminosities (see, e.g., [6]), and these quantities provide useful checks on the numerical quadratures. For example, after the merger, the tidal torque is absent and the equilibrium density profile is given by the familiar Shakura-Sunyaev result ([34]; see also [23, 24, 35] and references therein) for a thin disk around a single black hole remnant,

$$\begin{aligned} \nu\Sigma &= (\nu\Sigma)_{\rm out} \frac{\left(1 - r_{\rm isco}^{1/2}/r^{1/2}\right)}{\left(1 - r_{\rm isco}^{1/2}/r_{\rm out}^{1/2}\right)}, \quad [{\rm post-merger}] \\ &= \frac{\dot{M}}{3\pi}\left(1 - r_{\rm isco}^{1/2}/r^{1/2}\right). \end{aligned} \tag{31}$$

The corresponding luminosity is given by

$$\begin{aligned} L &= \frac{\dot{M}M}{2r_{\rm isco}}\left(1 - 3\frac{r_{\rm isco}}{r_{\rm out}} + 2\frac{r_{\rm isco}^{3/2}}{r_{\rm out}^{3/2}}\right), \quad [{\rm post-merger}] \\ &= \frac{\dot{M}M}{2r_{\rm isco}}, \quad r_{\rm out}\to\infty. \end{aligned} \tag{32}$$

3. Structure Equation: Nondimensional Units and Scaling

To solve Eq. (13) in steady state for general cases, and to help identify scaling behavior, it is convenient to introduce the following nondimensional variables:

$$\begin{aligned} s &= (r/r_{\rm out})^{1/2}, \quad s_1 = (a/r_{\rm out})^{1/2}, \quad s_2 = (r_{\rm isco}/r_{\rm out})^{1/2}, \\ \bar{\Sigma} &= \Sigma/\Sigma_{\rm out}, \quad \bar{\nu} = \nu/\nu_{\rm out}, \quad y = s\bar{\Sigma}, \quad \bar{y} = \bar{\nu} y, \\ \bar{h} &= h/r, \quad \tau = t/2t_{\rm vis}(r_{\rm out}), \quad \dot{m} = \dot{M}/(3\pi\nu_{\rm out}\Sigma_{\rm out}). \end{aligned} \tag{33}$$

In terms of these variables, equation (13) becomes

$$\frac{\partial y}{\partial \tau} = \frac{1}{s^2}\frac{\partial^2(\bar{\nu}y)}{\partial s^2} - \frac{1}{s^2}\frac{\partial}{\partial s}\left\{g^*(s) y \left[\frac{1}{\max(|s^2 - s_1^2|, s^2\bar{h})}\right]^4\right\}, \tag{34}$$

where

$$g = \frac{2}{3}\frac{f q^2 M^{1/2} r_{\rm out}^{1/2}}{\nu_{\rm out}} \tag{35}$$

and where

$$g^*(s) = \left\{ \begin{array}{ll} g s_1^8 & s > s_1 \\ -g s^8 & s < s_1 \end{array}\right. . \tag{36}$$

Evaluating Eq. (34) in steady state yields the second-order ODE

$$\frac{d^2}{ds^2}(\bar{\nu}y) - \frac{d}{ds}\left\{g^*(s)\left[\frac{1}{\max(|s^2 - s_1^2|, s^2\bar{h})}\right]^4 y\right\} = 0\ , \tag{37}$$

which must be solved for $s \in [s_2, 1]$ subject the boundary conditions

$$\text{b.c.'s}: \quad y = \bar{y} = \left\{ \begin{array}{ll} 1, & s = 1 \\ 0, & s = s_2 \end{array}\right. . \tag{38}$$

Equation (37) admits a first integral, just as in Eq. (16), so that we need only solve the first-order ODE

$$\frac{d\bar{y}}{ds} - f(s)\bar{y} = \dot{m}\ , \tag{39}$$

where

$$f(s) = \frac{g^*(s)}{\bar{\nu}(s)}\left[\frac{1}{\max(|s^2 - s_1^2|, s^2\bar{h})}\right]^4 . \tag{40}$$

III. STRUCTURE EQUATION: STEADY-STATE SOLUTION

A. General Solution

To solve Eq. (39) we introduce the function

$$F(s) = \int_s^1 f(s') ds'. \tag{41}$$

The ODE can be rewritten as

$$\frac{d}{ds}\left(e^F \bar{y}\right) = \dot{m} e^F, \tag{42}$$

and is readily integrated to give

$$\bar{y}(s) = e^{-F(s)}\left[b - \dot{m}\int_s^1 e^{F(s')} ds'\right]\ . \tag{43}$$

The boundary condition $\bar{y}(1) = 1$ gives $b = 1$, while the condition $\bar{y}(s_2) = 0$ gives

$$\dot{m} = \left[\int_{s_2}^1 e^{F(s)} ds\right]^{-1}\ . \tag{44}$$

Hence the solution is

$$y(s) = \frac{e^{-F(s)}}{\bar{\nu}(s)} \left[1 - \dot{m} \int_s^1 e^{F(s')} ds'\right] . \quad (45)$$

To compute $\dot{m}$ and $y(s)$ numerically, it is convenient to introduce the function

$$G(s) = \int_s^1 e^{F(s')} ds' . \quad (46)$$

Functions F and G satisfy the coupled ODEs

$$F'(s) = -f(s), \quad (47)$$
$$G'(s) = -e^{F(s)}, \quad (48)$$

with the initial conditions $F(1) = G(1) = 0$. Equations (44) and (45) can be written as

$$\dot{m} = \frac{1}{G(s_2)} , \quad (49)$$
$$y(s) = \frac{e^{-F(s)}}{\bar{\nu}(s)} \left[1 - \frac{G(s)}{G(s_2)}\right] . \quad (50)$$

In some cases, $G(s)$ may become large when s approaches s_1. To treat this complication we introduce the function $H(s) = \ln[G(s)]$, which satisfies the ODE

$$H'(s) = \frac{G'(s)}{G(s)} = -e^{F(s)-H(s)} . \quad (51)$$

In practice, the coupled ODEs (47) and (48) are integrated from $s = 1$ to $s = s^*$, where $s_1 < s^* < 1$. Then Eqs. (47) and (51) are integrated from $s = s^*$ to $s = s_2$ with the initial condition $H(s^*) = \ln[G(s^*)]$. Having computed the functions F and H for $s \in [s_2, 1]$, $\dot{m}$ and $y(s)$ are obtained by

$$\dot{m} = e^{-H(s_2)} , \quad (52)$$
$$y(s) = \frac{e^{-F(s)}}{\bar{\nu}(s)} \left[1 - e^{H(s)-H(s_2)}\right] . \quad (53)$$

We shall study the solution by numerically integrating the above equations for different choices of parameters in Section III B 4 below.

B. Limiting Cases and Asymptotic Behavior

Before obtaining numerical solutions for general cases it is instructive to evaluate Eq. (39) analytically for the disk structure in limiting regimes. We first observe that the parameter g defined in Eq.(35) may be evaluated as

$$g = 2\pi f q^2 \left(\frac{t_{\rm vis}}{t_{\rm orb}}\right)_{\rm out} \quad (54)$$

where we have used Eqs. (1) and (2). We also find it useful to introduce another nondimensional parameter

$$\tilde{g} = \frac{2\pi f q^2}{2\bar{h}^3} \left(\frac{t_{\rm vis}}{t_{\rm orb}}\right)_{r=a} = \frac{f q^2 M^{1/2} a^{1/2}}{3\nu(a)(h/a)^3}. \quad (55)$$

The physical meaning of $\tilde{g}$ can be understood as follows. Consider a ring of disk material of width h near $r = a$. The tidal torque action on the ring is [see Eq. (11)] $T_d(a) \approx 2\pi\Lambda\Sigma a h$. The viscous torque is $T_{\rm vis}(a) = -2\pi a^3 \nu(a)\Sigma\partial_r\Omega_K(a)$ [see Eq. (10)]. Hence

$$\frac{T_d(a)}{T_{\rm vis}(a)} \sim \frac{2h|\Lambda(a)|}{3\nu(a)} \left(\frac{a}{M}\right)^{1/2} = \tilde{g}. \quad (56)$$

The parameter $\tilde{g}$ therefore measure the relative importance of the tidal to viscous torques at $r = a$: when $\tilde{g}$ is small the tidal torque is unimportant, otherwise it plays a significant role. The variables f, q and $\bar{h}$ in Eq. (55) are each always less than unity, while the ratio $t_{\rm vis}/t_{\rm orb}$ is always larger than unity; hence $\tilde{g}$ can vary between zero and infinity, depending on the model (the same conclusion also applies to the parameter g).

1. Negligible Tidal Torques

In the limiting regime $\tilde{g} \to 0$ tidal torques are negligible and Eq. (39), may be solved together with boundary conditions (38) to yield

$$\bar{y} = \dot{m}(s - s_2), \quad (g = 0), \quad (57)$$

and

$$\dot{m} = \frac{1}{1 - s_2} . \quad (58)$$

Restoring units, Eqs. (57) and (58) translate to

$$\nu\Sigma = \frac{\dot{M}}{3\pi} \left[1 - r_{\rm isco}^{1/2}/r^{1/2}\right] \quad (59)$$

and

$$\frac{\dot{M}}{3\pi(\nu\Sigma)_{\rm out}} = \frac{1}{1 - r_{\rm isco}^{1/2}/r_{\rm out}^{1/2}} = 1, \quad r_{\rm out} \to \infty, \quad (60)$$

respectively. As expected, when tidal torques arising from the companion are negligible, Eqs. (59) and (60) reduce to Eq. (31), the quasistationary profile and accretion rate for a disk around a single black hole.

2. Strong Tidal Torques

In another limiting regime $\tilde{g} \gg 1$, tidal torques are strong and we will see in the following analysis that the accretion is shut off.

In the thin-disk limit $\bar{h} \to 0$, the function $f(s)$ changes from a large negative value to a large positive value at $s = s_1$. The function $F(s)$ defined in Eq. (41) thus has a narrow peak near $s = s_1$. Hence we may approximate $\dot{m}$ in Eq. (44) by integrating e^F over the small region

around $s = s_1$ where $|f(s)|$ reaches maximum. We first approximate $f(s)$ near $s = s_1$ by a step function

$$f(s) \approx \begin{cases} \frac{2\tilde{g}}{s_1\bar{h}}, & s_1 < s < s^+, \\ -\frac{2\tilde{g}}{s_1\bar{h}}, & s^- < s < s_1, \end{cases}, \tag{61}$$

where $s^+ = s_1/\sqrt{1-\bar{h}} \approx s_1(1+\bar{h}/2)$ and $s^- = s_1/\sqrt{1+\bar{h}} \approx s_1(1-\bar{h}/2)$. Using Eq. (41) we find

$$F(s) \approx F_1 + \tilde{g}\left(1 - \left|\frac{2(s-s_1)}{s_1\bar{h}}\right|\right) \quad \text{for } s^- < s < s^+, \tag{62}$$

where

$$\begin{aligned} F_1 &= \int_{s^+}^{1} f(s)ds \\ &\sim \frac{gs_1^8}{\bar{\nu}(s_1)}\int_{s^+}^{1}\frac{ds}{(s^2-s_1^2)^4} \\ &= \frac{\tilde{g}}{3}[1+O(\bar{h})]. \end{aligned} \tag{63}$$

The accretion rate $\dot{m}$ can then be approximated by

$$\begin{aligned} \frac{1}{\dot{m}} &\sim \int_{s^-}^{s^+} e^{F(s)}ds, \\ &\sim e^{\tilde{g}/3}\int_{s^-}^{s^+} ds\, \exp\left[\tilde{g}\left(1-2\left|\frac{s-s_1}{s_1\bar{h}}\right|\right)\right], \\ &= \frac{s_1\bar{h}}{\tilde{g}}e^{\tilde{g}/3}\left(e^{\tilde{g}}-1\right). \end{aligned} \tag{64}$$

For $e^{\tilde{g}} \gg 1$, we have

$$\dot{m} \sim \frac{\tilde{g}}{s_1\bar{h}}e^{-4\tilde{g}/3}. \tag{65}$$

Hence when the tidal torques are strong, the accretion is shut off. Our numerical calculation confirms that Eq. (65) is accurate when $e^{\tilde{g}} \gg 1$ and $\bar{h} \ll 1$.

In Sec. III B 1, we see that $\dot{m} \approx 1$ for weak tidal torques ($\tilde{g} \ll 1$). The above analysis shows that $\dot{m} \approx 0$ for strong tidal torques ($e^{\tilde{g}} \gg 1$). The critical transition between these two regimes occurs at $\tilde{g} = \tilde{g}_c$, which can be estimated by the condition

$$\frac{\tilde{g}_c}{s_1\bar{h}}e^{-4\tilde{g}_c/3} \sim 1. \tag{66}$$

For $a = 100M$, $r_{\rm out} = 10^5 M$ ($s_1 = 10^{-3/2}$) and $\bar{h} = 0.1$, Eq. (66) gives $g_c \sim 6$. We find in Sec. III B 4 below that $\tilde{g}_c$ lies between 5 and 10 for a power law viscosity $\nu(r) \propto r^n$, which is consistent with this simple analysis.

The density profile in the strong tidal torque regime is very different from that in the weak tidal torque regime. We will see in Sec. III B 3 below that in the asymptotic region in which $r \gg a$, the density profile is given by

$$\Sigma(r) \approx \Sigma_{\rm out}\frac{\nu_{\rm out}}{\nu(r)}\left(\frac{r}{r_{\rm out}}\right)^{-1/2} = \Sigma_{\rm out}\left(\frac{r}{r_{\rm out}}\right)^{-(n+1/2)} \tag{67}$$

for a power law viscosity. To estimate Σ near $r = a$, we first note from Eq. (48) that $G(s) < G(s_2)$ for $s > s_2$ ($r > r_{\rm ISCO}$). Hence $y(s) < e^{-F(s)}/\bar{\nu}(s)$. For $s^- < s < s^+$, Eqs. (62) and (63) give

$$\frac{\Sigma(r)}{\Sigma_{\rm out}} < \frac{1}{s\bar{\nu}(s)}\exp\left\{-\tilde{g}\left[\frac{4}{3} - \left|\frac{2(s-s_1)}{s_1\bar{h}}\right|\right]\right\} \ll 1 \tag{68}$$

for large $\tilde{g}$. For $s < s^-$, we combine Eqs. (46), (49) and (50) to write

$$y(s) = \frac{\dot{m}}{\bar{\nu}(s)}\int_{s_2}^{s} e^{F(s')-F(s)}ds'. \tag{69}$$

It follows from Eqs. (47), (40) and (36) that $F(s') - F(s) < 0$ for $s' < s < s_1$. Hence

$$\frac{\Sigma(r)}{\Sigma_{\rm out}} < \dot{m}\left(\frac{r}{r_{\rm out}}\right)^{-n}\left(1-\sqrt{\frac{r}{r_{\rm isco}}}\right) \ll 1 \quad (r < a) \tag{70}$$

for small $\dot{m}$ (large $\tilde{g}$).

We therefore see that the density plummets for $r \lesssim a$ when the tidal torques are strong. This behavior can be understood as follows. The tidal torque T_d pushes the disk matter radially outwards for $r > a$ and inwards for $r < a$; whereas the viscous torque $T_{\rm vis}$ always drags the matter inwards. The tidal torques are strongest near $r = a$, which tend to suppress the inflow and create a gap there. When T_d is sufficiently strong, the inflow is strongly suppressed near $r = a$. Inside the binary's orbit ($r < a$), both T_d and $T_{\rm vis}$ push matter inwards, so that when T_d is strong matter cannot accumulate in the inner region. Hence in steady state, there is practically no inner disk and the density of the outer disk near $r = a$ is also very small.

3. Asymptotic Behavior

As shown above, when tidal torques are present, the accretion rate may be much lower than the value quoted in Eqs. (58) and (60) for accretion onto a single black hole. The rate $\dot{m}$ depends sensitively on $\tilde{g}$ and requires the full numerical solution to determine accurately. But in the asymptotic region $r \gg a$ it is always possible to express the disk structure in terms of $\dot{m}$ even when tidal torques are present, as we now show.

Whenever $1 \geq s \gg s_1$, Eqs. (39) and (40) reduce to

$$\frac{d\bar{y}}{ds} - \frac{g}{\bar{\nu}}\left(\frac{s_1}{s}\right)^8\bar{y} = \dot{m}\ . \tag{71}$$

Consider the asymptotic regime where

$$\frac{gs}{\bar{\nu}}\left(\frac{s_1}{s}\right)^8 \ll 1, \tag{72}$$

in which case the second term in Eq. (71) is typically much less than the first term and therefore can be dropped. The solution to the resulting equation is

$$\bar{y} \approx \dot{m}s + 1 - \dot{m}, \tag{73}$$

or

$$\nu\Sigma \approx (\nu\Sigma)_{\rm out}\left[\dot{m}+(1-\dot{m})\left(\frac{r}{r_{\rm out}}\right)^{-1/2}\right], \qquad (74)$$

where we have used the boundary condition $\bar{y}(1)=1$ (Eq. 38). As we have argued in Sec. III B 2, whenever the tidal torque parameter satisfies $\tilde{g}\lesssim\tilde{g}_c$ we have $\dot{m}\approx 1$, while whenever $\tilde{g}\gtrsim\tilde{g}_c$ we have $\dot{m}\ll 1$. Not surprisingly, whenever tidal torques are unimportant, the asymptotic density profile reflected by Eqs. (73) and (74) is the same as the asymptotic profile given by Eqs. (57) and (59) (i.e., $\nu\Sigma\approx$ *constant* $\approx(\nu\Sigma)_{\rm out}\approx\dot{M}/3\pi$), but has a very different fall-off otherwise.

As an application, take the disk viscosity to be a power-law profile,

$$\nu(r)\propto r^n, \quad n\neq -7/2, \qquad (75)$$

or $\bar{\nu}(s)=s^{2n}$ with $n\neq -7/2$. Then Eq. (71) becomes

$$\frac{d}{ds}\left[q(s)\bar{y}\right]=q(s)\dot{m}\ , \qquad (76)$$

where

$$q(s)=\exp\left[\frac{g}{(2n+7)s^{2n-1}}\left(\frac{s_1}{s}\right)^8\right]. \qquad (77)$$

Consider the asymptotic region where

$$\frac{g}{(2n+7)s^{2n-1}}\left(\frac{s_1}{s}\right)^8\ll 1, \qquad (78)$$

or

$$s\gg\left(\frac{gs_1^{2n-1}}{2n+7}\right)^{1/(2n+7)}s_1\ . \qquad (79)$$

For example, if $n=1/2$, our fiducial case below, Eq. (79) reduces to

$$s\gg\left(\frac{g}{8}\right)^{1/8}s_1\ . \qquad (80)$$

In the asymptotic region defined by Eq. (79), $q(s)\approx 1$ and Eq. (76) again can be integrated to give Eq. (73), which now yields

$$\frac{\Sigma}{\Sigma_{\rm out}}=\frac{\bar{y}(s)}{s^{2n+1}}\approx\dot{m}\left(\frac{r}{r_{\rm out}}\right)^{-n}+(1-\dot{m})\left(\frac{r}{r_{\rm out}}\right)^{-(n+1/2)}. \qquad (81)$$

4. *Numerical Integrations*

Here we adopt the numerical recipe outlined in Section III A to evaluate the quasistationary density profile for different disk parameters. We adopt a power law viscosity $\nu(r)\propto r^n$. We note that in their vertically-integrated hydrodynamical simulations ref. [12] adopts $n=1/2$ for the value of the viscosity power-law index, while in their integrations of the radial secular evolution equations ref. [9] adopts $n=3/2$, while ref. [7] considers $n=0.4$ and $n=0.065$. In principle, the viscosity dependence, as well as the disk thickness, can be determined self-consistently once a viscosity law is adopted (e.g. an α-disk prescription). But due to the uncertainty in this law, we treat these as free parameters and postpone a self-consistent calculation for a future investigation.

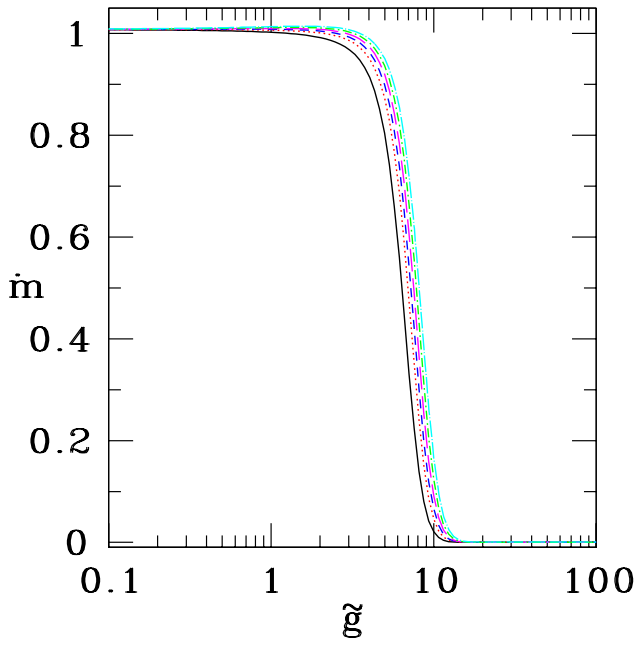

FIG. 1: Accretion rate $\dot{m}$ as a function of the tidal torque parameter $\tilde{g}$ for various values of the viscosity power-law index $-1\leq n\leq 2$. Results are shown for binary orbital radius $a=100M$, disk thickness $h/r=0.1$ in the vicinity of the disk edge at $r\approx a$ (see Eq. 12), disk outer radius $r_{\rm out}=10^5M$ and disk ISCO at $r_{\rm isco}=6M$. Solid (black) line represents the case for $n=-1$, dotted (red) line for $n=0$, dashed (blue) line for $n=1/2$, long-dashed (magenta) line for $n=1$, dot-dashed (green) line for $n=3/2$ and dot-long-dashed (cyan) line for $n=2$.

In Fig. 1 we show the dependence of the accretion rate $\dot{m}=\dot{M}/(3\pi\nu_{\rm out}\Sigma_{\rm out})$ on the strength of the tidal torque parameter $\tilde{g}$ defined in Eq. (55) for fixed binary radius $a=100M$, disk thickness $h/r=0.1$ and disk outer-radius $r_{\rm out}=10^5M$. In Fig. 2, we show the $\tilde{g}$ dependence of $\dot{m}$ for $n=1/2$ and $n=3/2$ and for various values of disk thickness h/r between 0.01 and 0.15, keeping other parameters fixed.

The key result emerging from these two figures is that for small tidal torques $\tilde{g}\lesssim\tilde{g}_c$ the accretion rate is very close to the rate onto an isolated black hole for the same asymptotic disk parameters, while for strong torques $\tilde{g}\gtrsim\tilde{g}_c$, it is sharply reduced. This behavior is predicted from the simple analysis in Secs. III B 1 and III B 2. Since the parameter $\tilde{g}$ varies as q^2, the accretion rate thus de-

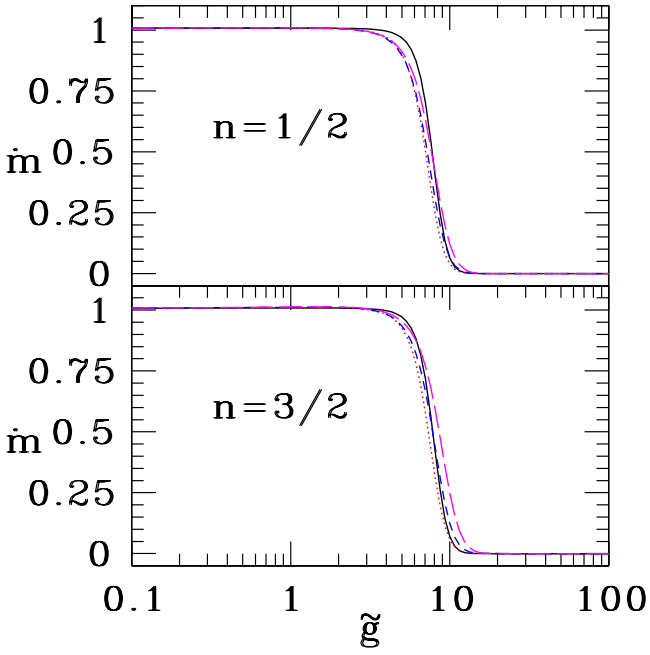

FIG. 2: Accretion rate $\dot{m}$ as a function of the tidal torque parameter $\tilde{g}$ for various values of disk thickness h/r. Results are shown for the viscosity power-law index $n = 1/2$ (*top*) and $n = 3/2$ (*bottom*), with binary orbital radius $a = 100M$, disk outer radius $r_{\rm out} = 10^5 M$ and disk ISCO at $r_{\rm isco} = 6M$. Solid (black) line represents the case for $h/r = 0.01$, dotted (red) line for $h/r = 0.05$, dashed (blue) line for $h/r = 0.1$, and long-dashed (magenta) line for $h/r = 0.15$.

creases as the binary mass ratio increases. If we define $\tilde{g}_c$ to be the value of $\tilde{g}$ so that $\dot{m} = 0.5$, we find $\tilde{g}_c$ lies between 5 and 10 for all the cases considered here, which is consistent with the value 6 estimated in Sec. III B 2.

In Fig. 3 we show the surface density profile for different tidal torque strengths $\tilde{g}$, fixing the viscosity index to $n = 1/2$, disk thickness $h/r = 0.1$, binary separation $a = 100M$ and $r_{\rm out} = 10^5 M$. It is evident from the figure that when the tidal torque is large and $\tilde{g} \gtrsim 5$, an appreciable gap develops in the density profile at the orbital radius of the secondary near $r = a$. Moreover, the gap widens and the density inside the gap falls off sharply as $\tilde{g} \gtrsim 15$. By contrast, when the tidal torque is small and $\tilde{g} \lesssim 5$, the gap shrinks and the density profile approaches the stationary profile around a single black hole of the same mass as the binary (Eq. 59). We thus find explicitly that the stationary solution yields an *inner* as well as an *outer* disk for sufficiently weak tidal torques (e.g., binaries with small q) and hardly any inner disk for strong tidal torques (e.g., binaries with large q), as predicted in Sec. III B 2. Correlating the values of $\dot{m}$ with the density profiles for Σ for each value of $\tilde{g}$ shows that the asymptotic profiles plotted in Fig. 3 agree with those derived in Eq. (81).

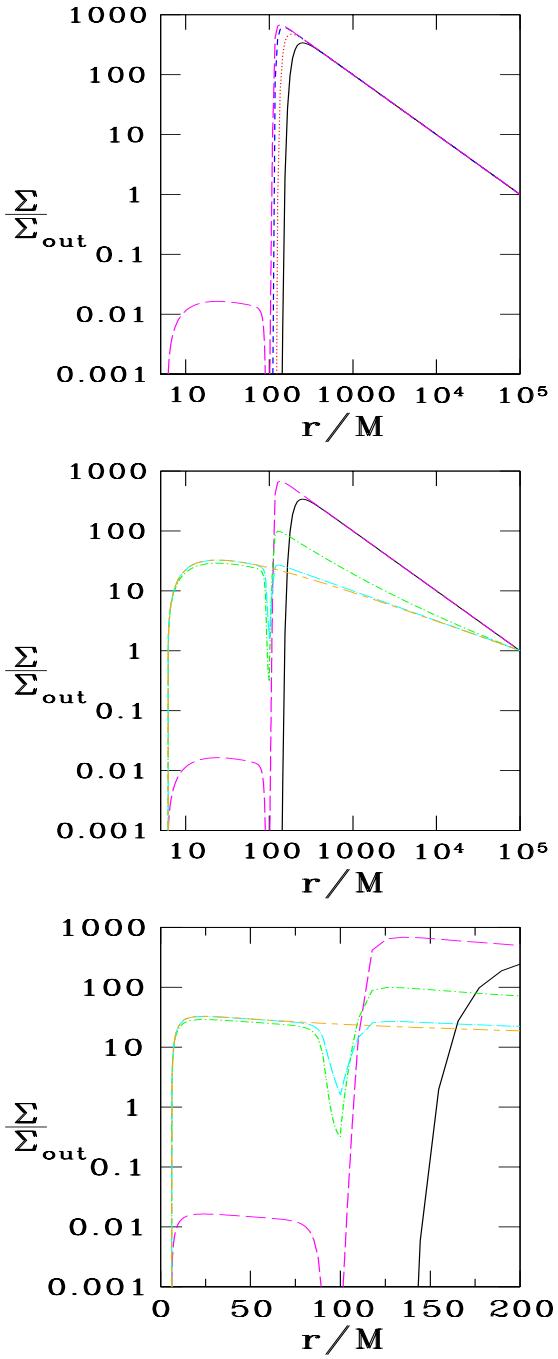

FIG. 3: The surface density profile Σ plotted for different values of the tidal torque parameter $\tilde{g}$. All results assume $h/r = 0.1$, $n = 1/2$, $a = 100M$, $r_{\rm out} = 10^5 M$ and $r_{\rm isco} = 6M$. *Top*: $\tilde{g} = 5000$ (black solid line), $\tilde{g} = 500$ (red dotted line), $\tilde{g} = 50$ (blue short-dash line) and $\tilde{g} = 15$ (magenta long-dash line). *Middle*: $\tilde{g} = 5000$ (black solid), $\tilde{g} = 15$ (magenta long-dash line), $\tilde{g} = 5$ (green dot-short-dash line), $\tilde{g} = 2.5$ (cyan dot-long-dash line), and $\tilde{g} = 0$ (orange long-dash-short-dash line). *Bottom*: Same as the middle figure but plotted in linear scale in r/M.

IV. ELECTROMAGNETIC SPECTRUM

Here we compute the (approximate) electromagnetic spectra from stationary disks for some representative, astrophysically plausible systems. We are particularly interested in probing disks at the time of decoupling and immersed in gaseous regions that will yield stationary post-merger accretion rates onto the *remnant* black hole near the Eddington limit. After decoupling, our stationary disk solution is no longer valid. To specify a model we first choose the parameters $M, q, a/M, r_{\rm out}/M \gg 1$ and n. We determine the decoupling separation a_d by the condition $t_{\rm GW}(a_d) = \beta t_{\rm vis}(2a_d)$ (setting $\beta = 0.1$), which yields

$$\left(\frac{a_d}{M}\right)^2 = \frac{128M\beta\zeta}{15\nu(2a_d)} = \frac{128M\beta\zeta}{15\nu_{\rm out}}\left(\frac{r_{\rm out}}{2a_d}\right)^n \qquad (82)$$

or

$$\frac{a_d}{M} = \left[\frac{128M\beta\zeta}{15\nu_{\rm out}}\left(\frac{r_{\rm out}}{2M}\right)^n\right]^{1/(n+2)}. \qquad (83)$$

We next set $\bar{h} = h/r = 0.1$ for the disk thickness near $r = a$. To establish the scale for the density and disk size in physical units we fix $\Sigma_{\rm out}$ and $r_{\rm out}$, which determines the disk mass $M_{\rm disk}$. Finally, we determine $\nu_{\rm out}$ by specifying the accretion rate onto the black hole remnant, $\dot{M}_{\rm rem} = 3\pi\nu_{\rm out}\Sigma_{\rm out}$ (see Eq. 60 in the limit $r_{\rm isco}/r_{\rm out} \ll 1$) to be a fraction γ of the Eddington value, whereby

$$\gamma \equiv \frac{\dot{M}_{\rm rem}}{\dot{M}_{\rm Edd}} = \frac{3\pi\nu_{\rm out}\Sigma_{\rm out}}{\dot{M}_{\rm Edd}}, \qquad (84)$$

which gives

$$\nu_{\rm out} = \frac{16\gamma M m_p}{\sigma_T \Sigma_{\rm out}}. \qquad (85)$$

The above choices determine the torque parameters g and $\tilde{g}$ according to Eqs. (35) and (55), setting $f = 0.01$. These choices specify a unique, albeit approximate, model for a stationary Newtonian disk about a binary black hole system and determine the disk surface density and the gas accretion rate. Given such a model, the electromagnetic spectrum can be computed following the prescription outlined in Section II B 2 above.

A. Numerical Integrations

We illustrate the calculation by considering a binary black hole with a $10^8 M_\odot$ primary. We take the viscosity power-law index to be $n = 0.5$, and set $r_{\rm out} = 10^3 M$, $\gamma = 0.1$, and $\Sigma_{\rm out} = 1.5 \times 10^4 {\rm g\,cm^{-2}}$. The decoupling separation a_d is calculated from Eq. (83). Our choice of parameters gives $M_{\rm disk} \sim 10^3 M_\odot$ for $0 \le q \le 0.1$ (see Table I), which is much smaller than the mass of the secondary BH for $q > 10^{-3}$. These values for the disk density and mass are comparable to those considered in [9, 10]. We evaluate the disk profiles and electromagnetic structure for different choices of mass ratio $q \le 0.1$. Table I summarizes our results. Scaling behavior for different choices of binary and disk parameters is presented in Appendix A. We see that the decoupling separation $a_d \propto \zeta^{0.4}$ [see Eq. (83)] increases from $9.6M$ for $q = 10^{-3}$ to $56M$ for $q = 0.1$. The accretion rate drops rapidly towards 0 when $q > 2\times10^{-3}$, which corresponds to $\tilde{g} > 6.5$, and is consistent with Fig. 1.

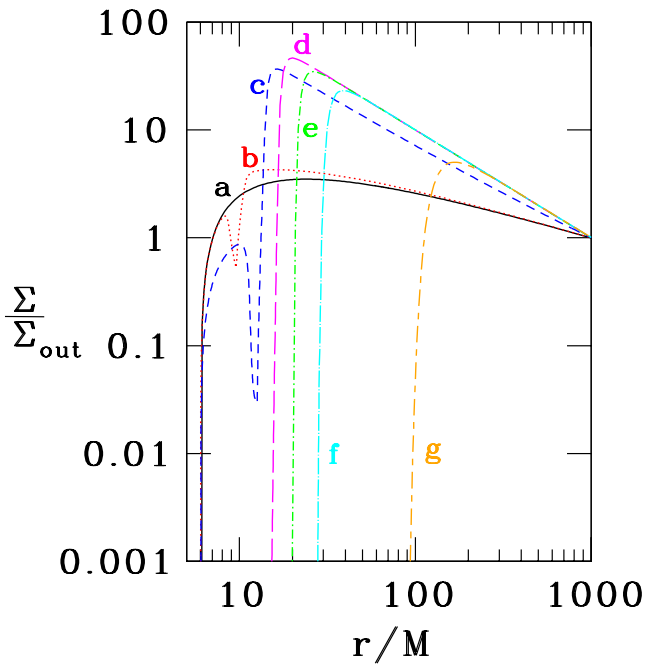

FIG. 4: Surface density of disks around a binary black hole just before decoupling. Shown here are cases for the binary mass ratios (a) $q = 0$ (black solid line), (b) $q = 10^{-3}$ (red dotted line), (c) $q = 2 \times 10^{-3}$ (blue short-dash line), (d) $q = 3 \times 10^{-3}$ (magenta long-dashed line), (e) $q = 5 \times 10^{-3}$ (green dot-short-dash line), (f) $q = 10^{-2}$ (cyan dot-long-dash line), and (g) $q = 10^{-1}$ (orange long-dash-short-dash line).

Figure 4 shows the surface density of the disk for different values of q. As in Fig. 3, for small q, there is a dip near $r = a$ in the density profile, but an inner disk of substantial density is present. When $q > 2 \times 10^{-3}$, the accretion rate drops to a small value and Σ falls sharply near $r = a$, leaving essentially no inner disk. We also see that the density in the asymptotic region changes from r^{-1} for small $\dot{m}$ (large q) to $r^{-1/2}$ for substantial $\dot{m}$ (small q), as predicted by Eq. (81). For a fixed $\Sigma_{\rm out}$, the steeper decrease of density in the small accretion cases ($q > 2 \times 10^{-3}$) give larger Σ in the asymptotic region, which results in a larger disk mass as shown in Table I. However, as q increases further, the decoupling radius a_d moves to a larger radius so that the inner radius of the disk moves out as well. This behavior leads to the small decrease in disk mass for $q > 10^{-2}$ as shown in Table I.

TABLE I: Properties of disks around a binary black hole at the decoupling separation. The mass of the primary black hole is set to $M = 10^8 M_\odot$, outer disk radius $r_{\rm out} = 10^3 M$, surface density $\Sigma_{\rm out} = 1.5 \times 10^4 {\rm g\,cm^{-2}}$ and the Eddington parameter $\gamma = 0.1$.

Case	q	$\tilde{g}$	$t_{\rm orb}$(days)	t_{GW}(yrs)	a_d/M	$M_{\rm disk}(M_\odot)$	$\dot{m}$	$\dot{M}(M_\odot\,{\rm yr}^{-1})$	$L({\rm erg\,s}^{-1})$
a	0	0	–	–	–	660	1.08	0.29	1.3×10^{45}
b	10^{-3}	1.6	1.1	10	9.6	670	1.07	0.29	1.8×10^{45}
c	2×10^{-3}	6.5	1.6	16	12.6	880	0.41	0.11	1.4×10^{46}
d	3×10^{-3}	14	2.0	20	14.8	1000	3.2×10^{-4}	8.6×10^{-5}	1.5×10^{46}
e	5×10^{-3}	39	2.8	27	18.2	1000	1.8×10^{-15}	4.9×10^{-16}	1.1×10^{46}
f	10^{-2}	160	4.2	40	23.9	1000	0	0	6.6×10^{45}
g	10^{-1}	16000	15	145	56.0	880	0	0	1.4×10^{45}

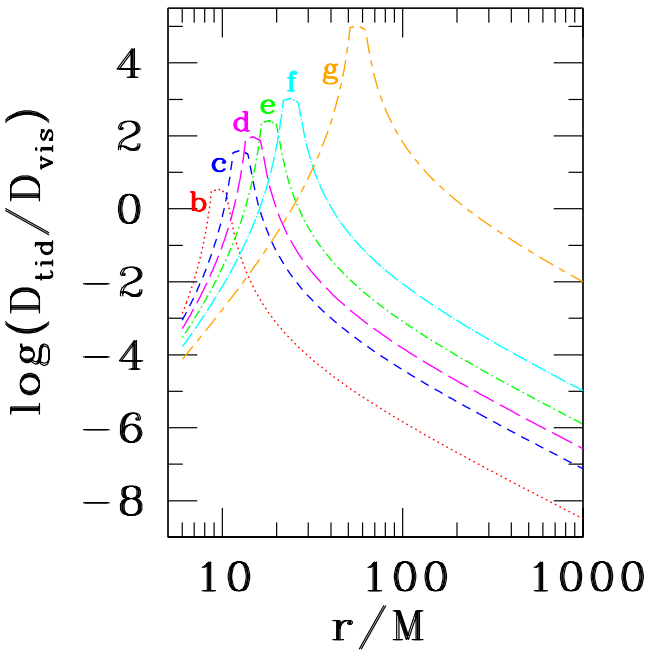

FIG. 5: Ratio of tidal heating to viscous heating $D_{\rm tid}/D_{\rm vis}$ as a function of radius for disks around a binary black hole just before decoupling for binary ratios (b) $q = 10^{-3}$ (red dotted line), (c) $q = 2 \times 10^{-3}$ (blue short-dash line), (d) $q = 3 \times 10^{-3}$ (magenta long-dashed line), (e) $q = 5 \times 10^{-3}$ (green dot-short-dash line), (f) $q = 10^{-2}$ (cyan dot-long-dash line), and (g) $q = 10^{-1}$ (orange long-dash-short-dash line).

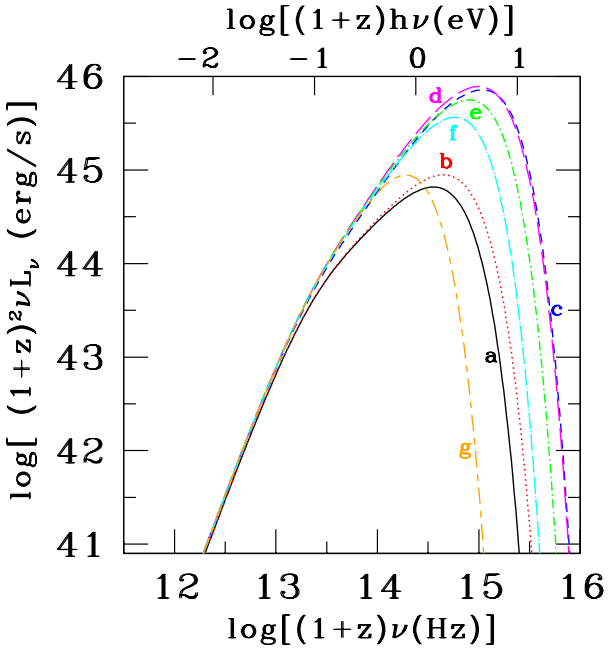

FIG. 6: Electromagnetic spectrum of disks around a binary black hole at redshift z just before decoupling. Shown here are cases for the binary mass ratios (a) $q = 0$ (black solid line), (b) $q = 10^{-3}$ (red dotted line), (c) $q = 2 \times 10^{-3}$ (blue short-dash line), (d) $q = 3 \times 10^{-3}$ (magenta long-dashed line), (e) $q = 5 \times 10^{-3}$ (green dot-short-dash line), (f) $q = 10^{-2}$ (cyan dot-long-dash line), and (g) $q = 10^{-1}$ (orange long-dash-short-dash line). Note that lines (c) and (d) are barely distinguishable.

Figure 5 shows the ratio of tidal heating to viscous heating $D_{\rm tid}/D_{\rm vis}$ as a function of radius for each case. In all cases with $q \neq 0$, the effect of tidal heating dominates over the viscous heating at radius $r \sim a$, but decreases rapidly both at larger and smaller radii. This result is expected since the tidal torque is created by the gravitational force of the secondary black hole, which decreases with the distance from the secondary. It can be proven easily from Eqs. (20), (22), (11) and (12) that $D_{\rm tid}/D_{\rm vis} \sim r^3|\Lambda|/\nu$. Hence $D_{\rm tid}/D_{\rm vis}$ has a peak near $r = a$, $D_{\rm tid}/D_{\rm vis} \sim r^{3/2}/(r-a)^4$ for $r \gtrsim a$ and $D_{\rm tid}/D_{\rm vis} \sim r^{11/2}/(r-a)^4$ for $r \lesssim a$.

Figure 6 shows the electromagnetic spectrum of the disk for each value of q. We see that the luminosity increases substantially at first as q increases above zero and the accretion rate $\dot{m}$ drops. This is due to the large increase in Σ as shown in Fig. 4. The peak frequency also shifts to a higher value because the enhanced viscous and tidal dissipation give rise to higher temperatures in the disk. For $q \gtrsim 3 \times 10^{-3}$, however, the tidal torque of the binary becomes large enough to expel the disk material inside its orbit and shut off the accretion. As a result, the

edge of the disk moves to a larger radius where the temperature is lower. This effect shifts the peak frequency back to a lower value. Since a large fraction of the electromagnetic radiation comes from the innermost part of the disk where the temperature is high, the disk luminosity drops when $q \gtrsim 3\times10^{-3}$ (see Table I), as the inner edge of the disk moves to a larger radius. We see from Table I that the total luminosity of the disk for $q = 0.1$ drops to about the same value as the standard Shakura-Sunyaev disk.

Most noteworthy is the fact that even as the gas accretion rate is shut off by the companion, tidal heating serves to maintain a high luminosity from the disk, comparable in magnitude to the luminosity from a single black hole. For high q cases in which there is no inner disk, the luminosity plummets after decoupling over a timescale $t_{\rm GW}$, as the inspiral accelerates and tidal heating drops. Later on the luminosity from the disk about the remnant then increases on a slow viscous timescale, as the outer disk diffuses inward [1, 6, 7]. This luminosity achieves values comparable to those prior to decoupling, but at higher frequency, since the main radiation region outside the inner edge of the disk moves inward from a_d to $r_{\rm isco}$, where temperatures become hotter. For low q cases in which there is a substantial inner disk the change in luminosity and the frequency spectrum following decoupling is much less pronounced.

Periodicities in the luminosity are expected on an orbital timescale during the inspiral. This timescale is on the order of days at decoupling for the cases considered here (see Table I).

Figure 6 indicates that most of the radiation emitted by the disk at decoupling is in visible and near infrared wavelengths. For a source at redshift $z = 1$, the apparent magnitude is about 19 and radiated in infrared wavelength. Assuming the disk is not obscured by interstellar dust, it could be observable by the James Webb Space Telescope (JWST) and Large Synoptic Survey Telescope (LSST).

V. SUMMARY

We have studied the effects of tidal torque on a quasistationary disk around a binary black hole with small binary mass ratio before decoupling. We find that the density profile and accretion rate is sensitive to the mass ratio q through the tidal torque parameter $\tilde{g}$ defined by Eq. (55). For small $\tilde{g}$, the density profile and accretion rate are slightly modified from the standard Shakura-Sunyaev disk. Specifically, the density inside the binary orbit ($r < a$) is smaller than the standard Shakura-Sunyaev disk but is about the same in the outer region. A substantial drop in density is seen near $r = a$ due to the strong tidal torque in that region. As $\tilde{g}$ increases, the tidal torque becomes stronger and the density in the inner disk, as well as the accretion rate, decrease further. On the other hand, the density in the outer disk increases and a gap (inside of which the density is much smaller) develops between the inner and outer disk. The gap widens with increasing $\tilde{g}$. When $\tilde{g}$ exceeds a critical value $\tilde{g}_c$, the tidal torque is strong enough to effectively expel the material inside and near the binary orbit and practically shuts off accretion. The asymptotic density profile also changes [see Eq. (81)]. For a power law viscosity $\nu \propto r^n$, the critical value is $\tilde{g}_c \sim 7$ and depends weakly on the index n and disk thickness h/r (see Figs. 1 and 2).

We compute the luminosity and electromagnetic spectrum emitted by the disk due to viscous heating and tidal dissipation at the time of decoupling. The results are summarized in Table I and Fig. 6 for disks surrounding a primary black hole of mass $M = 10^8 M_\odot$, outer disk radius $r = 10^3 M$, surface density $\Sigma_{\rm out} = 1.5\times10^4 {\rm g\,cm^{-2}}$, and the Eddington parameter $\gamma = 0.1$. The disk luminosity at first increases with q. This is caused by the increase in density of the outer disk. The radiation also shifts to higher frequencies, as the enhanced viscous and tidal heating give rise to higher disk temperatures. The disk luminosity reaches a maximum near $q = 3\times10^{-3}$, when the accretion is shut off by the strong tidal torques. When $q > 3\times10^{-3}$, the decoupling binary separation a_d moves to a larger radius. The strong tidal torque expels disk material inside and near the binary orbit, causing the radiation region to move to larger radii, where the temperatures are lower. The disk luminosity drops and the radiation shifts to a lower frequency. We note that even as the gas accretion rate is shut off by the companion, tidal heating serves to maintain a high luminosity from the disk, comparable in magnitude to the luminosity from a single black hole. Most of the radiation is emitted in the near infrared and visible wavelength and may exhibit periodicities on the binary orbital timescale. For a source at redshift $z = 1$, the apparent magnitude is about 19 (provided the disk is not obscured by the interstellar dust) and could be detected by JWST and LSST.

Acknowledgments: It is a pleasure to thank C. Gammie for useful discussions. This paper was supported in part by NSF Grants PHY06-50377 and PHY09-63136 and NASA Grants NNX07AG96G and NNX10A173G to the University of Illinois at Urbana-Champaign.

Appendix A: Scaling in disk radiation

In this appendix, we rewrite the equations in Sec. II B 2 in terms of the nondimensional variables introduced in Sec. II B 3 and then establish scaling relations in terms of the mass of the primary black hole M and the Eddington parameter γ.

We first rewrite Eq. (20) as

$$D_{\rm vis}(t,r) = \frac{9}{8}\frac{\nu_{\rm out}\Sigma_{\rm out}M}{r_{\rm out}^3}\left(\frac{\bar{y}}{s^7}\right) \ . \qquad \text{(A1)}$$

The torque function Λ can be written as

$$\Lambda = \frac{3\nu_{\rm out}\sqrt{M}}{4r_{\rm out}^{3/2}s^2} f(s)\bar{\nu}(s). \quad \text{(A2)}$$

Hence the rate of change in binary binding energy is [see Eq. (21)]

$$\begin{aligned}\dot{E}_{\rm tid} &= \frac{3\pi M\sqrt{r_{\rm out}}\nu_{\rm out}\Sigma_{\rm out}}{a^{3/2}}\int_{s_2}^{1} f(s)\bar{y}(s)ds \\ &= \frac{3\pi M\sqrt{r_{\rm out}}\nu_{\rm out}\Sigma_{\rm out}}{a^{3/2}}[1-\dot{m}(1-s_2)]\ . \quad \text{(A3)}\end{aligned}$$

The tidal torque density Eq. (11) becomes

$$\frac{\partial T_d}{\partial r} = \frac{3\pi\Sigma_{\rm out}\nu_{\rm out}}{2}\sqrt{\frac{M}{r_{\rm out}}}\,\frac{f(s)\bar{y}(s)}{s}, \quad \text{(A4)}$$

Consider the expression

$$\begin{aligned}\int_{r_{\rm isco}}^{r_{\rm out}} dr|dT_d/dr| &= 2r_{\rm out}\int_{s_2}^{1} s|dT_d/dr|ds \\ &= 3\pi\Sigma_{\rm out}\nu_{\rm out}\sqrt{Mr_{\rm out}}\left[-\int_{s_2}^{s_1} f(s)\bar{y}(s)ds\right. \\ &\quad \left.+\int_{s_1}^{1} f(s)\bar{y}(s)ds\right] \\ &= 3\pi\Sigma_{\rm out}\nu_{\rm out}\sqrt{Mr_{\rm out}}\times \\ &\quad [1-2\bar{y}(s_1)+\dot{m}(2s_1-s_2-1)]. \quad \text{(A5)}\end{aligned}$$

Hence Eq. (22) becomes

$$D_{\rm tid} = \frac{3M\nu_{\rm out}\Sigma_{\rm out}[1-\dot{m}(1-s_2)]}{8(r_{\rm out}a)^{3/2}[1-2\bar{y}(s_1)+\dot{m}(2s_1-s_2-1)]}\frac{|f(s)|\bar{y}(s)}{s^3}. \quad \text{(A6)}$$

The total dissipation rate is

$$\begin{aligned}D &= D_{\rm tid}+D_{\rm vis} \\ &= \frac{3M\nu_{\rm out}\Sigma_{\rm out}}{8r_{\rm out}^3}\bar{D}(s), \quad \text{(A7)}\end{aligned}$$

where

$$\bar{D}(s) = \left[\frac{3\bar{y}}{s^7}+\frac{1-\dot{m}(1-s_2)}{1-2\bar{y}(s_1)+\dot{m}(2s_1-s_2-1)}\frac{|f(s)|\bar{y}(s)}{s^3s_1^3}\right]. \quad \text{(A8)}$$

The temperature ratio is given by

$$\left(\frac{T_*}{T_s}\right)^4 = \frac{D}{3M\dot{M}_{\rm rem}/8\pi r_{\rm isco}^3} = \frac{3}{s_2^6}\bar{D}(s). \quad \text{(A9)}$$

Gathering all the relevant formulae, the accretion rate, luminosity, and disk mass can be expressed in cgs units as follows:

$$\dot{M} = 0.27M_\odot\,{\rm yr}^{-1}\left(\frac{\gamma}{0.1}\right)\left(\frac{M}{10^8M_\odot}\right)\dot{m}, \quad \text{(A10)}$$

$$L_\nu = 1.99\times10^{30}{\rm erg}\left(\frac{\gamma}{0.1}\right)^{3/4}\left(\frac{M}{10^8M_\odot}\right)^{5/4} f^*(\nu/\nu_*), \quad \text{(A11)}$$

$$\nu_* = 2.91\times10^{14}\left(\frac{\gamma}{0.1}\right)^{1/4}\left(\frac{M}{10^8M_\odot}\right)^{-1/4}{\rm Hz}, \quad \text{(A12)}$$

$$L = 1.26\times10^{45}\bar{L}\left(\frac{\gamma}{0.1}\right)\left(\frac{M}{10^8M_\odot}\right){\rm erg\ s^{-1}}, \quad \text{(A13)}$$

$$\bar{L} \equiv 2s_2^2\int_{s_2}^{1}\bar{D}(s)ds, \quad \text{(A14)}$$

and

$$M_{\rm disk} = 2.06\times10^3M_\odot\left(\frac{\Sigma}{1.5\times10^4{\rm g\,cm^{-2}}}\right)\left(\frac{r_{\rm out}}{10^3M}\right)^2\times\left(\frac{M}{10^8M_\odot}\right)^2\int_{s_2}^{1}s^{2-2n}\bar{y}ds. \quad \text{(A15)}$$

[1] M. Milosavljević and E. S. Phinney, ApJL **622**, L93 (2005).
[2] E. M. Rossi, G. Lodato, P. J. Armitage, J. E. Pringle, and A. R. King, ArXiv e-prints (2009), 0910.0002.
[3] J. D. Schnittman and J. H. Krolik, Astrophys. J. **684**, 835 (2008).
[4] L. R. Corrales, Z. Haiman, and A. MacFadyen, ArXiv e-prints (2009), 0910.0014.
[5] S. M. O'Neill, M. C. Miller, T. Bogdanović, C. S. Reynolds, and J. D. Schnittman, Astrophys. J. **700**, 859 (2009).
[6] S. L. Shapiro, Phys. Rev. D **81**, 024019 (2010), 0912.2345.
[7] T. Tanaka and K. Menou, Astrophys. J. **714**, 404 (2010), 0912.2054.
[8] T. Tanaka, Z. Haiman, and K. Menou, Astron. J. **140**, 642 (2010), 1004.5411.
[9] P. J. Armitage and P. Natarajan, ApJL **567**, L9 (2002).
[10] P. Chang, L. E. Strubbe, K. Menou, and E. Quataert, Mon. Not. R. Astro. Soc. pp. 1003–+ (2010), 0906.0825.
[11] B. D. Farris, Y. T. Liu, and S. L. Shapiro, Phys. Rev. D **81**, 084008 (2010), 0912.2096.
[12] A. I. MacFadyen and M. Milosavljević, Astrophys. J. **672**, 83 (2008).
[13] M. Megevand, M. Anderson, J. Frank, E. W. Hirschmann, L. Lehner, S. L. Liebling, P. M. Motl, and D. Neilsen, Phys. Rev. D **80**, 024012 (2009), 0905.3390.
[14] B. D. Farris, Y. T. Liu, and S. L. Shapiro, in preparation .
[15] T. Bode, R. Haas, T. Bogdanović, P. Laguna, and D. Shoemaker, Astrophys. J. **715**, 1117 (2010).
[16] M. Anderson, L. Lehner, M. Megevand, and D. Neilsen, Phys. Rev. D **81**, 044004 (2010).
[17] T. Bogdanovic, T. Bode, R. Haas, P. Laguna, and

D. Shoemaker, ArXiv e-prints (2010), 1010.2496.
[18] There are exceptions, as in the case of nearly equal-mass binaries at merger, when abrupt mass loss and recoil due to gravitational wave emission occurs [2, 4, 5, 36] .
[19] F. K. Liu, X.-B. Wu, and S. L. Cao, Mon. Not. R. Astro. Soc. **340**, 411 (2003).
[20] P. Artymowicz and S. H. Lubow, Astrophys. J. **421**, 651 (1994).
[21] D. Lynden-Bell and J. E. Pringle, Mon. Not. R. Astro. Soc. **168**, 603 (1974).
[22] N. J. Turner, ApJL **605**, L45 (2004), arXiv:astro-ph/0402539.
[23] J. E. Pringle, A&A **19**, 137 (1981).
[24] J. Frank, A. King, and D. J. Raine, *Accretion Power in Astrophysics* (Cambridge University Press, Cambridge, 2002).
[25] P. Goldreich and S. Tremaine, Astrophys. J. **241**, 425 (1980).
[26] K. Hourigan and W. R. Ward, Icarus **60**, 29 (1984).
[27] W. R. Ward, Icarus **126**, 261 (1997).
[28] D. N. C. Lin and J. Papaloizou, Astrophys. J. **309**, 846 (1986).
[29] P. Chang, Astrophys. J. **684**, 236 (2008), 0801.2133.
[30] C. M. Hirata, ArXiv e-prints (2010), 1010.0758.
[31] C. M. Hirata, ArXiv e-prints (2010), 1010.0759.
[32] Accounting for the dominance of electron scattering over free-free absorption opacity in the hottest region leads to a higher surface temperature by the well-known ratio $(\kappa_{\rm es}/\kappa_{\rm ff})^{1/8} \sim$ few, and this, in turn, results in a higher thermal photon energy [1, 7, 34, 35, 37] .
[33] From the context it should not be difficult to distinguish the photon frequency ν from the viscosity ν.
[34] N. I. Shakura and R. A. Sunyaev, A&A **24**, 337 (1973).
[35] I. D. Novikov and K. S. Thorne, in *Black Holes, Les Houches*, edited by C. Dewitt and B. DeWitt (Gordon and Breach, New York, 1973), pp. 343–450.
[36] N. Bode and S. Phinney, 2007, in APS Meeting, http://meetings.aps.org/link/BAPS.2007.APR.S1.10 .
[37] S. L. Shapiro and S. A. Teukolsky, *Black Holes, White Dwarfs, and Neutron Stars: The Physics of Compact Objects* (John Wiley, New York, 1983).